Advances in Data Science and Adaptive Analysis
Vol. 10, No. 2 (2018) 1840008 (30 pages)

DOI: 10.1142/S2424922X18400089.

World Scientific
www.worldscientific.com

Continuous Estimation Prediction of Knee Joint Angles Using Fusion of Electromyographic and Inertial Sensors for Active Transfemoral Leg Prostheses

Alberto López-Delis*

Department of Electrical Engineering
University of Brasilia, Brasilia-DF, Brazil

Medical Biophysics Center, University of Oriente
Santiago de Cuba, Cuba
lopez.delis69@gmail.com

Cristiano J. Miosso

Biomedical Engineering Graduate Program
University of Brasilia, Gama, Brasilia-DF, Brazil
cristiano.jacques@gmail.com

João L. A. Carvalho†, Adson F. da Rocha‡
and Geovany A. Borges§

Department of Electrical Engineering
University of Brasilia, Brasilia-DF, Brazil
†*joaoluiz@gmail.com*
‡*adsonr@gmail.com*
§*gaborges@unb.br*

Accepted 11 May 2018
Published 8 August 2018

Information extracted from the surface electromyographic (sEMG) signals can allow for the detection of movement intention in transfemoral prostheses. The sEMG can help estimate the angle between the femur and the tibia in the sagittal plane. However, algorithms based exclusively on sEMG information can lead to inaccurate results. Data captured by inertial-sensors can improve this estimate. We propose three myoelectric algorithms that extract data from sEMG and inertial sensors using Kalman-filters. The proposed fusion-based algorithms showed improved performance compared to methods based exclusively on sEMG data, generating improvements in the accuracy of knee joint angle estimation and reducing estimation artifacts.

Keywords: Electromyographic; inertial-sensors; fractal dimension; slope sign changes; waveform length; cepstral analysis; data fusion; Kalman-filter.

*Corresponding author.

1. Introduction

Several research groups have developed electronic systems for controlling joints. These devices include, for instance, electromechanical knees, which use some form of computational intelligence to control the resistive torque around the knees. Grimes *et al.* [1977] developed an echo control scheme for gait control, in which a modified knee trajectory is deduced from the healthy leg and played back on the contralateral side. Popovic *et al.* [1995] presented a battery-powered active knee joint actuated by direct current (DC) motors, controlled by a finite state knee controller that uses a robust position tracking algorithm for gait control. Some companies have also developed electronic knees for clinical use. For example, the Otto Bock C-leg [Kastner *et al.* (1999)] provides adjustable resistance for flexion and extension in the swing using onboard intelligence and a particular software package. Sup *et al.* [2008] introduced a finite-state machine for a knee ankle prosthesis with pneumatic actuators. The stiffness and damping parameters of the impedance controller can take different values according to four gait states: stance flexion/extension, pre-swing, swing flexion, and swing extension. A variant of prosthesis equipped with electric actuators and a unidirectional series spring is presented in [Sup *et al.* (2008a)]. In this system, a load cell in series with each actuator controls the force. The performance was evaluated with test with healthy subjects on a treadmill. The gait patterns generated with the prototype was similar to those found in experiments with healthy people with a healthy gait.

A pattern-recognition-based myoelectric control algorithm is typically composed of various main modules; a data segmentation stage handles the data before feature extraction, to improve precision and response time. A feature extraction stage preprocesses the data for reducing the amount of information to be analyzed. Linear or nonlinear transformation of the original data can allow for the acquisition of new variables (features). The central component is the neural network classifier, which must be capable of learning relations between the input features and the desired control outputs. Significant advancements in pattern recognition methodology are in progress. A common approach is to extract parameters from the data, such as time-domain features (e.g. mean absolute value, waveform length, number of zero crossings) [Kelly *et al.* (1990); Hudgins *et al.* (1993)], spectral parameters (e.g. auto-regressive model) [Huang *et al.* (2005); Hargrove *et al.* (2008)], time-frequency coefficients (e.g. short-time Fourier transform) [Englehart *et al.* (2001)] and time-scale coefficients (e.g. discrete wavelet transform and wavelet packet decomposition) [Englehart *et al.* (2001); Chu *et al.* (2005); Wang *et al.* (2006)]. Further data reduction may be achieved using a feature projection stage between pre-processing and classification [Englehart *et al.* (2001); Chu *et al.* (2005); Wang *et al.* (2006)]. This approach eliminates redundant information, which speeds up the training process. It may also help mapping the data into small and well-separated clusters, by absorbing signal variations and noise present in the data's original vector-space.

On the other hand, the problem of continuously predicting joint angles using surface electromyographic (sEMG) signals is comparatively underdeveloped [Smith *et al.* (2008); Ha *et al.* (2011)]. Surynarayanan and Reddy [1997] developed an intelligent system to detect the elbow joint angle from sEMG signals measured on the biceps and reported a maximum root mean squared (RMS) error on the order of 24%. Gupta and Reddy [1996] found a linear relationship between quasi-static index finger flexion angles and sEMG signals from the flexor digitorum superficialis muscle. Recently, Reddy *et al.* used myoelectric signals from the flexor muscle to control computer models of finger and wrist joints. Fakuda *et al.* [2003] developed a manipulator controlled by arm movements, using myoelectric signals to determine which joint should be controlled. Sawaguchi *et al.* [2011] developed estimation models of the wrist angle from the corresponding myoelectric potential. One of them is a one-link model considering the moment arm. The other is illustrated by a multi-body model with a half-moon shaped rigid body rolling inside a bowl-shaped body. Each model provided good estimation of the wrist angle from measured surface myoelectric potentials. Comparing the estimation accuracy for the two models, the half-moon-shaped model yield more accurate estimation. Zhang *et al.* [2012] presented an mth order nonlinear model to describe the relationship between the sEMG signals and the joint angles of human legs; in this method a simple Back Propagation (BP) neural network has been used for model estimation. The results showed that the proposed EMG-based method had a good performance for angle estimation for both able-bodied subjects and spinal cord injury patients; the average RMS error in angle estimation for leg extension exercises was less than 9°, and the average RMS error for treadmill exercise is less than 6° for all the able-bodied subjects. Yang *et al.* [2013] proposed a hierarchical projected regression method to allow for online estimation of the joint angle of the human elbow. Lizhi *et al.* [2014] established a state space model with an unknown structure, for estimation of the finger joint angle, which used time-domain features extracted from sEMG signals. Shengxin *et al.* [2017] applied a radial basic function (RBF) neural network to estimate the tremor in joint angle based on an estimate of the root mean square of sEMG. Tang *et al.* [2014] used the BP neural network to map the nonlinear relationship between sEMG and the elbow joint angle. In this type of myoelectric control, the level of muscle activity, either in isometric or isotonic contraction in a dynamic limb motion, is the most important process to be recognized [Ferreira *et al.* (2005)]. To evaluate this activity level, a combination of time domain and frequency domain features may provide improved estimation precision, in comparison with either approach independently. This feature combination is also computationally efficient, and is more robust to electrode displacement [Delis *et al.* (2009)].

We have proposed two different algorithms for estimating the intended knee joint angle from sEMG signals measured on upper-leg opposing muscles [Ferreira *et al.* (2005); Delis *et al.* (2009)]. The first method uses the autoregressive (AR) model for feature extraction and a Levenberg–Marquardt (LM) multi-layer perceptron neural network for supervised learning [Ferreira *et al.* (2005)]. The second method

uses time- and frequency-domain sEMG feature extraction (amplitude histogram and AR model, respectively), self-organizing maps for feature projection, and a LM neural classifier [Delis *et al.* (2009)]. However, myoelectric control methods that rely solely on sEMG signals may lead to significantly inaccurate knee joint angle estimates, for different reasons [Merletti and Parker (2009)]: (i) high level of amplification due to the typically low sEMG signal levels; (ii) failures due to broken electrode connections or sudden changes in the electrode–electrolyte interface due to poor contact; (iii) motion of the electrodes over the skin; and (iv) noise caused by the power supplies.

The previous results motivate the search for other types of sensors to be used in prostheses, which may potentially allow adaptations during its use by the patient. For example, microelectromechanical gyroscopes and joint motion sensors may allow for measuring the angular velocity of the knee joint. The integration of these data can be used to obtain an estimate of the knee joint angle, which can be used to make small corrections of the neural network coefficients in real-time. Fusion of the sEMG information with inertial sensor data could also improve the precision of the prosthesis control during movement, and thus provide a more reliable myoelectric control [Oskoei and Hu (2007)].

Data fusion is the continuous process of implementing a model of the domain of interest, using data from different types. Multisensor data fusion has found widespread use in diverse areas: industry, commerce, local robot guidance for global military defense, etc. [Luo *et al.* (2002)]. The purpose of data fusion is to produce an improved model or estimate of a system from a set of independent data sources. The use of range sensory data allows automatic extraction of information about the sensed environment under different operating conditions, which increases the performance, reliability, data rates, and autonomy of the estimation algorithm [Luo *et al.* (2002); Hall and Llinas (1997); Luo (1996)].

In many real-time applications, the desired model can be described with the use of state vectors that establish time dependence in dynamic processes [Diniz (1997)]. The combination of information from the sensors and subsequent estimation of the states should be done coherently to reduce the uncertainty about the actual states. The Kalman-filter is a state estimation algorithm widely used for optimally estimating the unknown state of a linear dynamic system from Gaussian-distributed noisy observations [Manyika and Durrant-Whyte (1994)]. The algorithm uses a predefined system model to predict the state at the next time step [Diniz (1997)].

The fusion of sEMG signals applications with other data is not common in the literature. However, a few groups have investigated this type of fusion. Silva *et al.* [2003], for example, applied data fusion of mechanomyography (MMG) signals for the generation of binary control signals for an electrically powered prosthesis. The goal was to implement a practical MMG-based muscle contraction detection system for prosthesis control. In this work, the MMG signals were recorded using silicon-embedded microphone-accelerometer sensor pairs. A multisensor data fusion

strategy then generated binary control signals, based on the RMS values of the segmented signals acquired with each transducer [Silva *et al.* (2003)]. The measured contraction detection accuracies were 95% and 86%, for the wrist extensors and the flexors, respectively. López *et al.* [2009], on the other hand, proposed two strategies for data fusion based on variance weighted average (VWA) and decentralized Kalman-filter (DKF), by means of an arrangement of redundant sEMG potentials. They estimated the muscle contraction amplitude and converted it to an angular reference used to control the robotic joint. The VWA and DFK algorithms provided satisfactory results, in the sense that the joint never moved beyond its safety range [López *et al.* (2009)]. Fan and Yin [2013] presented a healthcare technology for active and progressive early rehabilitation using multisource information fusion from surface electromyography and force-position extended physiological proprioception. The active-compliance control based on interaction force between patient and exoskeleton is applied to accelerate the recovery of the neuromuscular function. The Extended physiological proprioception (EPP) feedback system based on tactile stimuli is developed to help rebuild the closed-loop control system of human body. Preliminary experiments and clinical trial indicate the human-machine system can move coordinately, which demonstrates the feasibility, safety and effectiveness of the progressive exoskeleton-assisted training [Fan and Yin (2013)].

In this work, we propose three myoelectric algorithms based on the fusion of sEMG signals and inertial sensor data, for estimation of intended knee joint angle, which may potentially be used to control active transfemoral leg prostheses (Fig. 1). The proposed algorithms use a feature extraction stage where time domain methods (fractal dimension, slope sign changes and waveform length) and frequency domain methods (cepstral coefficients) are combined. Angular velocity information derived from a gyroscope is used to improve the angle estimation and to make the system more robust to artifacts. The first strategy uses an additional feature extraction stage based on Kalman-filters; in this step, the estimated angular velocity (from the gyroscopes) and the coefficients obtained by fractal dimension, slope sign changes, waveform length and cepstral coefficients are fused and used as the input vectors to the LM neural network to estimate the knee angle. The second strategy combines,

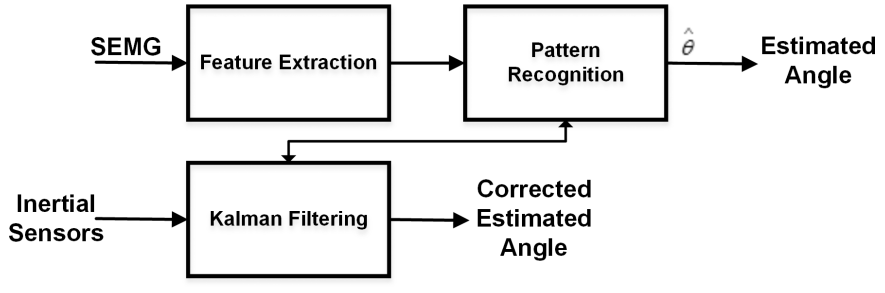

Fig. 1. General block diagram of the knee angle estimation algorithms proposals based on data fusion.

during the Kalman-filter's correction process, the angular velocity information and the knee angle estimated using the LM neural network. The filter output is the corrected estimated knee angle from the fusion process. The third strategy is a modification of the second procedure, and uses a compatibility test, based on the Mahalanobis distance, between the prediction and the correction processes of the Kalman-filter. This allows the algorithm to disregard sEMG data which are not coherent with a motion model (usually when artifacts are present).

The three proposed strategies aim to reduce potential artifacts that arise from the knee angles estimated by the LM neural network. We tested these methods using signals collected from twelve healthy volunteers. We then present quantitative and qualitative comparisons between the proposed approaches and previous estimation methods for knee joint angle, in terms of error-to-signal percentages, correlation coefficients and error event statistics. The experimental results suggest that strategies based on data fusion lead to improvements and better robustness to movement artifacts concerning the algorithms based solely on sEMG signals.

2. Materials and Methods

2.1. *Data acquisition and experimental protocol*

In order to evaluate the performance of the proposed algorithms, we collected signals from 12 healthy volunteers, using a microcontrolled bioinstrumentation system previously developed by our research group [Delis *et al.* (2009)]. This system analogically multiplexes two channels of amplified sEMG signal, the signal from the electrogoniometer, and the data from the gyroscope sensors. These signals are sampled using a 13-bit analog-to-digital converter, which is electrically isolated from the microcontroller and the power supply using an optocoupler and a DC–DC converter. During this procedure, data is transferred to a personal computer using a serial interface. We adopted a sampling rate of 1043.45 Hz per channel. To avoid aliasing and to eliminate DC components, analog filters limited the sEMG signals to the 20–500 Hz frequency range [SENIAM (2008)]. Also, a digital real-time adaptive notch filter reduced the 60 Hz power line interference [Ahlstrom and Tompkins (1985)].

To evaluate the robustness of the proposed methods, we also conducted two additional sets of tests. First, we acquired new sEMG signals, but we intentionally loosened the straps that hold the cables between the electrodes and the instrumentation equipment. The idea was to evaluate the robustness to movement artifacts, by comparing their influence on the knee joint angles estimated by the proposed fusion-based methods and on those estimated by the algorithms based solely on sEMG signals. The other set of tests involved evaluating the systems' robustness to 60 Hz interference. To assess this aspect, we added a 60 Hz signal with 0.1 mV amplitude to each sEMG channel (in choosing this magnitude, we adopted the maximum 60 Hz noise levels observed during the previous experiments, and kept them constant during the entire procedure).

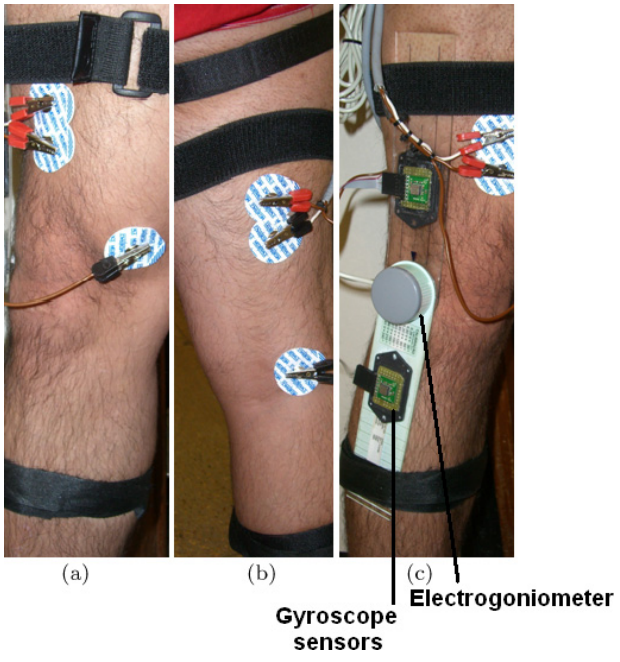

Fig. 2. Placement of: (a, b) sEMG electrodes, and (c) electrogoniometer and gyroscope sensors.

The experimental protocol was approved by the research ethics committee of the University of Brasília (process no. 079/09, group III). The volunteers provided informed consent and were studied in accordance with institutional policies. To collect the sEMG signals, we positioned two pairs of 10 mm Ag/AgCl surface electrodes using a bipolar configuration over a pair of antagonist muscles, corresponding, respectively, to the flexion and extension movements of the knee joint (Figs. 2(a) and 2(b)). The longitudinal axes of the electrodes were made parallel to the muscle's longitudinal axes, and the distance between the electrode pairs' centers was 2 cm, according to the SENIAM protocol recommendations [SENIAM (2008)]. The reference electrodes were placed over the lateralis and medialis epicondyles of femur, while an electrogoniometer was placed and strapped to the external side of the leg over the center of knee joint (Fig. 2(c)). The gyroscope sensors were placed over the thigh and shank (Fig. 2(c)). The difference between the signals measured by the gyroscopes reflects the angular velocity of the knee joint. Both inertial sensors were simultaneously-acquired with the sEMG signals.

For each volunteer, four 15-s measurements were performed on each day with 5-min rest intervals, over the course of five days. For each measurement, the subject was asked to walk in a particular direction at a constant pace. Some variability in pace was observed between measurements. The first and third measurements from each day were used for training, and the second and the fourth measurements were used for testing.

Figure 3 presents examples of simultaneously-acquired sEMG and inertial signals from a representative subject. A total of 240 measurements were obtained, with half of them being used for training and the other half being used for testing.

2.2. *Feature extraction*

In this work, we used cepstral coefficients for frequency-domain sEMG signature discrimination, and time domain feature vectors in the myolectric signal such as fractal dimension, slope sign changes, and waveform length. In this section, we briefly describe how we computed these sets of features, to use them as inputs to the supervised learning stages. Regarding the cepstral coefficients, consider, for example, a zero mean, discrete-time segment of signal s of length M, with discrete Fourier transform (DFT), here called S. Then, the cepstrum vector of the s segment is, by definition, the inverse DFT of the logarithm of the squared magnitude of S [Kang *et al.* (1995)], i.e.

$$c(m) = \frac{1}{M} \sum_{f=0}^{M-1} \log(|S(f)|^2) e^{j2\pi f m/M}, \quad \forall\, m \in \{0, 1, \ldots, M-1\}. \tag{1}$$

To compute the cepstral coefficients, we used an approach based on the AR signal model. Some works have reported that the AR-derived cepstrum feature has better performance than the unprocessed AR feature [Kang *et al.* (1995); Chiou *et al.* (2004)]. By computing the Laurent series [Kang *et al.* (1995)] for each coefficient in Eq. (1), we obtain the recursive relation:

$$\begin{aligned} c(0) &= -a_0, \\ c(m) &= -a_m - \sum_{i=0}^{m-1} \left(1 - \frac{m+1}{i+1}\right) a_m c_{m-i}, \quad \forall\, m \in \{1, 2, \ldots, K-1\}, \end{aligned} \tag{2}$$

where a_m is the mth order coefficient of the AR model associated with s. Using Eq. (2), we can compute the first K cepstral coefficients. Even though the cepstral coefficients are derived directly from the AR coefficients, they do not convey the same information, because the recursive operation changes the features distribution nonlinearly [Kang *et al.* (1995)]. We obtained the cepstral coefficients using a sixth-order AR model and the process described in Eq. (2). Regarding the time domain feature vectors, we focus in the following measures.

Fractal dimension (FD): It is a measure of muscle strength [Hu *et al.* (2005)]. Fractals refer to properties of objects or signal patterns that exhibit self-similarity over a range of magnification/scales and with the relationship that is fractional. FD is a measure of this relationship, defined as the change in length of the curve with the change in the measurement scale. FD is a measure of the source properties and is a measure of its complexity, spatial extent or its space-filling capacity and is related to shape and dimensionality of the process [Acharya *et al.* (2005)]. FD was calculated using Higuchi algorithm [Higuchi (1998)] for nonperiodic and irregular

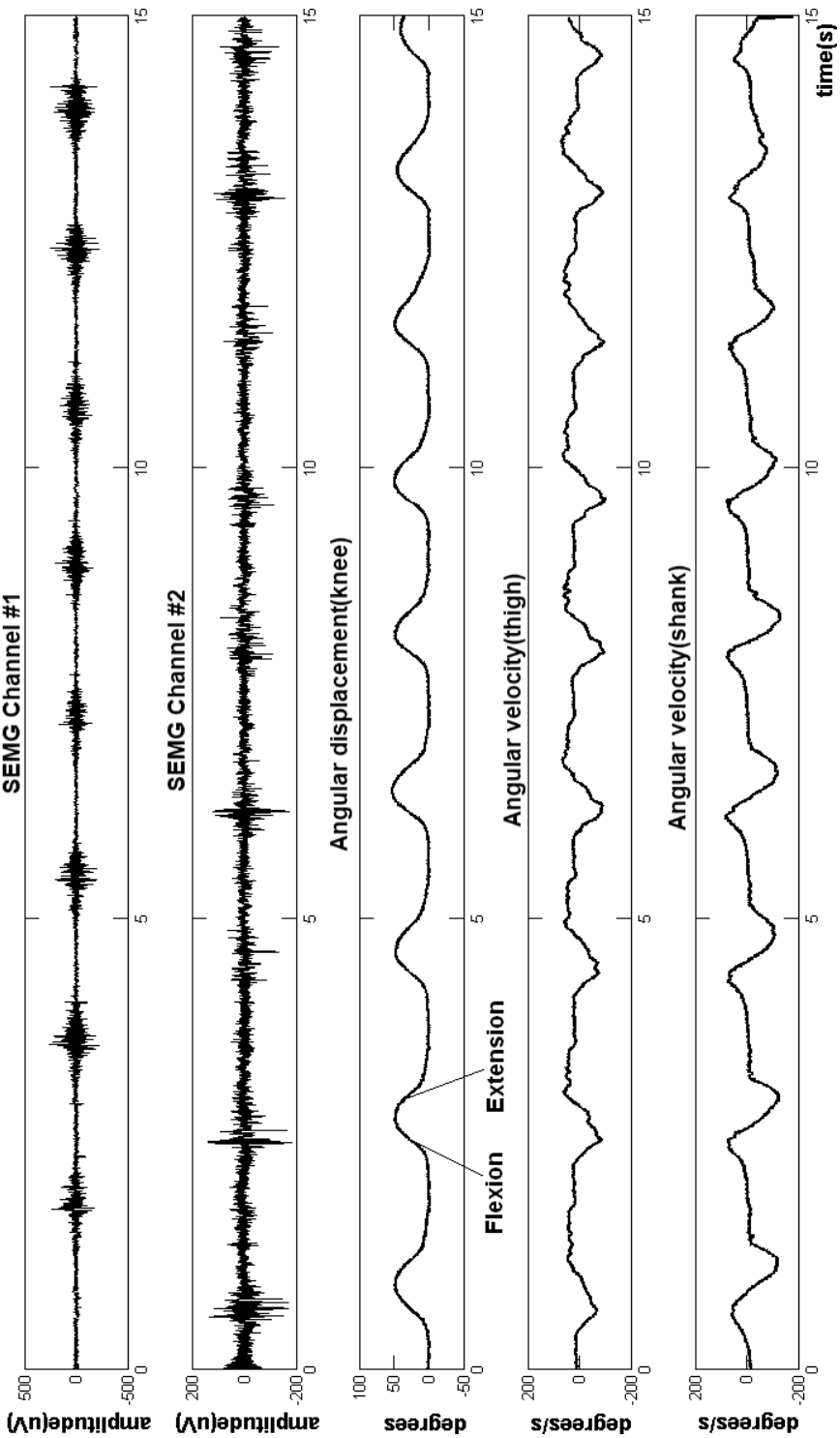

Fig. 3. Representative set of simultaneously acquired sEMG signals, electrogoniometer angles, and gyroscope measurements.

time series. This algorithm yields a more accurate and consistent estimation of FD for physiological signals than other algorithms [Esteller *et al.* (2001)].

Slopes sign changes (SSC): It is another method to represent frequency information of the sEMG signal, associated to the number of times that slope of the sEMG signal changes sign [Phinyomark *et al.* (2012)]. The number of changes between the positive and negative slopes among three sequential segments is measured using a threshold function, to avoiding background noise in the EMG signal. The suitable value for the threshold parameter is usually chosen within the interval from 50 μV to 100 mV [Phinyomark *et al.* (2012)].

Waveform length (WL): Is a measure of the complexity of the sEMG signal [Phinyomark *et al.* (2012)]. It is defined as cumulative length of the sEMG waveform over the time segment. Some articles in the literature called this feature as wavelength (WAVE) [Phinyomark *et al.* (2012)].

2.3. *Pattern classification*

After computing the signal features according to the previous section, we apply them to an LM multi-layer perceptron neural network [Hagan and Menhaj (1994)], to estimate the intended knee joint angle. Similarly, to the quasi-Newton methods, the LM neural network was designed to approach second-order training speed without computing the Hessian matrix. In fact, the critical step in the LM algorithm is the computation of the Jacobian matrix, which can be obtained using standard backpropagation techniques [Hagan and Menhaj (1994)]. Therefore, the resulting computational complexity is significantly lower than that required by the Hessian matrix computation. Although the computational requirements of the LM algorithm become much higher after each iteration, this is entirely compensated by its higher efficiency, especially when high precision is required. In applying the LM algorithm to the extracted features, we tested three fusion strategies, described next. These approaches combine these features with information from the gyroscopes, for increased accuracy.

2.4. *First data fusion strategy*

Figure 4 presents the block diagram for the proposed knee angle estimation algorithm using the first data fusion strategy. The use of angular velocity information from the gyroscopes improves angle estimation precision and reduces estimation artifacts. A Kalman-filter is applied directly to noisy gyroscopes measurements to estimate angular velocity. Note that the objective of Kalman-filters, generally speaking, is the estimation of the mean of nonstationary noisy signals, by minimizing the mean squared error (recursive least squares for stochastic models).

The estimated signal — the angular velocity, in our application — is modeled using a state-space formulation, describing its dynamical behavior [Diniz (1997)]

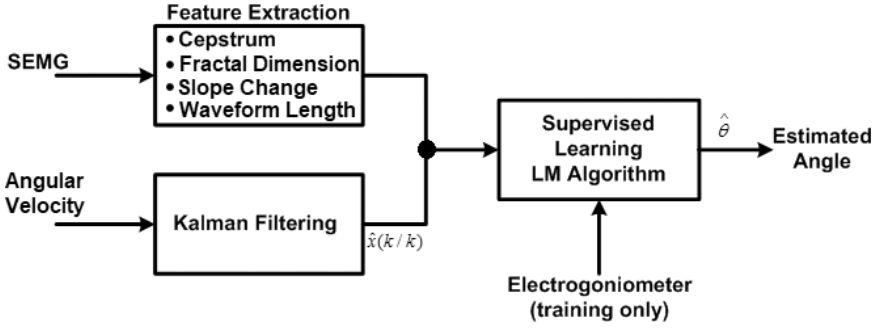

Fig. 4. Block diagram of the proposed knee angle estimation algorithm based on the first fusion strategy.

according to the linear stochastic model described by:

$$x(k) = x(k-1) + n(k) \tag{3}$$

and

$$y(k) = x(k) + v(k), \tag{4}$$

where $x(k)$ is the knee joint angular velocity at time k; $n(k)$ is the noise at time k, modeling the evolution of the joint angular velocity between two sampling intervals; $y(k)$ is the measured angular velocity at time k, obtained from subtracting the angular velocity values measured on the thigh and shank; and $v(k)$ is the measurement noise at time k. We assume that $n(k)$ and $v(k)$ have independent Gaussian distributions, with zero means, variances given by q^2 and r^2, respectively, and independent from $x(0)$. When applying the Kalman-filter to this model, the prediction process for each iteration cycle is given by:

$$\hat{x}(k/k-1) = \hat{x}(k-1) \tag{5}$$

and

$$P(k/k-1) = P(k-1) + q^2, \tag{6}$$

with the initialization $q^2 = 4$, $r^2 = 10$, $x(1) = 0$ and $P(1) = 0.01$.

The correction process, on the other hand, is given by

$$G_k = \frac{P(k/k-1)}{(P(k/k-1) + r^2)}, \tag{7}$$

$$\hat{x}(k/k) = \hat{x}(k/k-1) + G(k)(y(k) - \hat{x}(k/k-1)) \tag{8}$$

and

$$P(k) = (1 - G(k))P(k/k-1), \tag{9}$$

where $G(k)$ is the Kalman-filter gain at time k; $P(k)$ is the error covariance matrix associated with the estimation process; and $\hat{x}(k/k)$ is an optimal estimate of $x(k)$

in the least-squares sense. It is possible to show that, for this specific problem, this filter is equivalent to a unity-gain, low-pass, first-order filter, with time-varying cut-off frequency. This cut-off frequency is computed considering the noise variances q^2 and r^2, as well as the error variance associated with $\hat{x}(k/k)$ [Diniz (1997)]. The value of $\hat{x}(k/k)$ is an optimal estimate of the mean of the knee joint angular velocity at sampling step k. At each time instant, the angular velocity estimate $\hat{x}(k/k)$, along with the sEMG fractal dimension, slope sign changes, waveform length and cepstral coefficients, are used as inputs to the neural classifier, as shown in Fig. 2.

2.5. *Second data fusion strategy*

We also evaluated the use of information fusion in the correction stage of the Kalman-filter. The Kalman-filter can deal with disturbances originated from sEMG measurements and propagated to the neural network in a more sophisticated structure. This approach may reduce the effect of perturbations in the estimated angles provided by the neural network. Figure 5 presents the block diagram for this second data fusion strategy.

Note that the sEMG feature vectors are the inputs to the LM neural network. Then, the estimated knee joint angle is modeled using a state-space formulation, describing its dynamical behavior [Diniz (1997)], according to the linear stochastic model given by

$$x(k) = x(k-1) + T \cdot u(k) + n(k) \tag{10}$$

and

$$y(k) = x(k) + v(k), \tag{11}$$

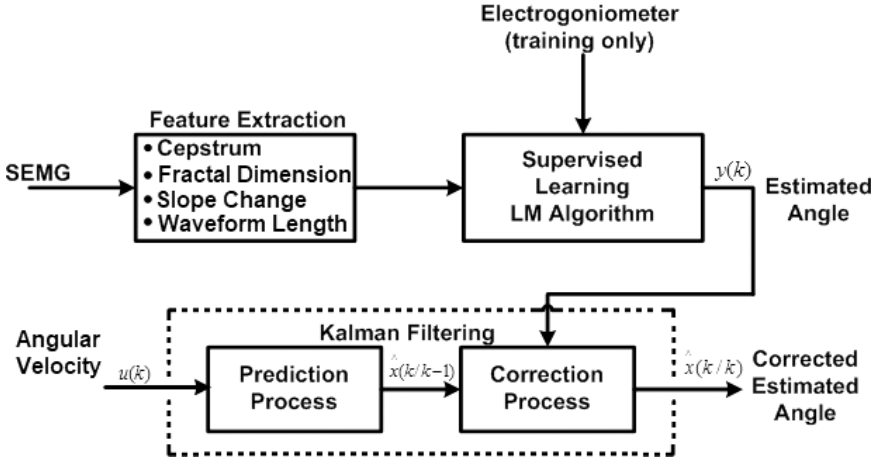

Fig. 5. Block diagram of the proposed knee angle estimation algorithm based on the second fusion strategy.

where $x(k)$ is the corrected estimated knee angle at time k; $u(k)$ is the measured angular velocity acquired at time k using a sampling period T(this angular velocity is obtained from subtracting the angular velocity values measured on the thigh and shank); $n(k)$ is noise at time k, modeling the evolution of the knee joint angle between two sampling intervals; $y(k)$ is the estimated knee joint angle at time k, obtained from the LM neural network output; and $v(k)$ is the measurement noise at time k.

Again, we assume that $n(k)$ and $v(k)$ are normally distributed with zero mean and variances given by q^2 and r^2, respectively; we also assume that $n(k)$ and $v(k)$ are independent. When applying the Kalman-filter to this model, the prediction process at each iteration cycle follows:

$$\hat{x}(k) = \hat{x}(k-1) + T \cdot u(k) \tag{12}$$

and

$$P(k/k-1) = P(k-1) + T^2 \cdot \sigma_{u_k}^2 + q^2, \tag{13}$$

with the initialization $q^2 = 4$, $r^2 = 10$, $x(1) = 0$, $\sigma_{u_k}^2 = 25$ and $P(1) = 0.0$, and where $\sigma_{u_k}^2$ is the sample variance of the measured angular velocity. As in the case of the first proposed fusion strategy, the correction process is given by Eqs. (7)–(9).

Note that the value of $\hat{x}(k/k)$ is an optimal estimate of the knee joint angle, as provided by the fusion process with the angular velocity information at time k and angular orientation estimate provided by the neural network applied to the sEMG data.

2.6. *Third data fusion strategy*

We also evaluated a modification of the previous strategy, based on a compatibility test using the Mahalanobis distance [De Maesschalck *et al.* (2000)]. The Mahalanobis distance is a useful way of determining the similarity of sample sets, and it is not dependent on the scale of the measurements.

The procedure proposed, shown in Fig. 6, uses the Mahalanobis distance's estimate after the prediction stage of the Kalman-filter, thus affecting the correction process. The goal is to filter possible artifacts that arise from the angle estimated by the LM neural network, at each time step of the data fusion process. Such artifacts are usually propagated as rapid changes in the LM neural network output, which become incompatible with the smooth motion of the knee joint.

When the Kalman-filter is applied to the linear stochastic models described by Eqs. (10) and (11), the prediction process follows Eqs. (12) and (13). We evaluate the square root Mahalanobis distance $d(x, y)$ between the estimated angle from the LM neural network, $y(k)$, and the previous corrected angle estimate, according to:

$$d(x,y) = \sqrt{\sum_{i=0}^{N-1} \frac{(y(k-i) - \hat{x}(k-i/k-i-1))^2}{r^2 + P(k-i/k-i-1)}} \tag{14}$$

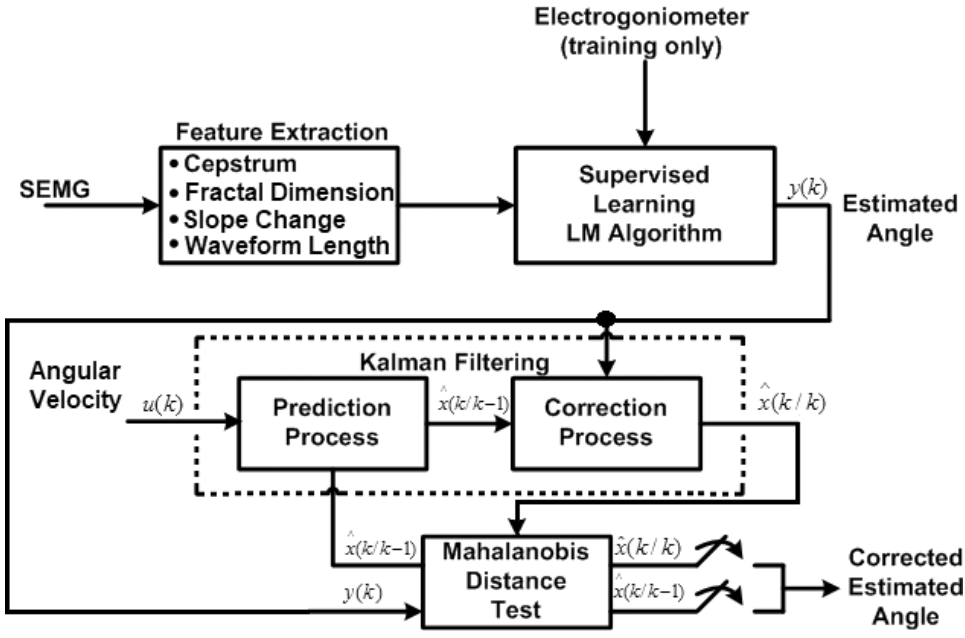

Fig. 6. Block diagram of the proposed knee angle estimation algorithm based on the third fusion strategy.

and use this distance in a decision process which is part of the calculation of a corrected estimate for $x(k)$, as follows:

$$\hat{x}(k/k) = \begin{cases} \hat{x}(k/k-1) + G(k)(y(k) - \hat{x}(k/k-1)) & \text{if } d(x,y) < th, \\ \hat{x}(k/k-1) & \text{otherwise,} \end{cases} \tag{15}$$

where th is a threshold value chosen based on a Chi-square distribution [Duda *et al.* (2000)], as we discuss below. The parameter N in Eq. (14) defines the length of the window for computing the Mahalanobis distance. For small N, the filter becomes very sensitive to nonGaussian noise in the measurements, which can lead the filter to disregard measurements provided by the LM neural network. On the other hand, large values of N can lead the system to take too long to make the estimate insensitive to the effect of an artifact. Based on these considerations, we empirically chose $N = 15$ (approximately 14 ms) in this work.

Note that the window length for feature extraction was much longer ($M = 200$). Feature extraction aims to associate fractal dimension, slope sign changes, waveform length and cepstral features with the knee angle. Thus, the dynamics of feature processing must be faster than the evolution of the knee angle. The feature extraction window must be long enough to guarantee a minimum number of representative samples, but short enough to ensure satisfactory temporal resolution for knee angle estimation. On the other hand, the window for Mahalanobis distance calculation

aims to compare a knee angle estimate with a set of model-based predicted values. If the estimate deviates considerably from a large number of predicted values within the window, we assume that we are dealing with an artifact, and hence we discard the estimated value and use the predicted value instead. Therefore, the window length N is associated with the maximum duration of an acceptable artifact. For example, if we consider as "acceptable" those artifacts which last only a few samples, then the estimates would not be discarded, and the model would follow these estimates. However, if the artifact lasts many samples, then the Mahalanobis distance would be large, allowing artifact detection. Also, the estimator would disregard the estimates from the neural network and would use predicted values until the estimated values normalize. This approach would minimize the effect of those "unacceptable" artifacts.

If $d(x, y) < th$, the correction process of the Kalman-filter is implemented according to Eqs. (7)–(9). At each iteration cycle, an optimal estimate of $x(k)$ that represents the knee joint angle from the fusion process with the angular velocity information is obtained. If $d(x, y) \geq th$, on the other hand, the estimate $x(k)$ is computed based on the previous estimated angle, preserving the prediction from possible artifacts associated with the angle estimate given by the neural network.

Now, assuming that the uncertainty on x and y is Gaussian with zero mean, $d^2(x, y)$ follows a χ^2_N distribution [De Maesschalck *et al.* (2000)]. For example, with $N = 15$, results are considered to be statistically similar (with 95% confidence) if $d^2 \leq 25$, which leads to $d(x, y) \leq 5$; thus, $th = 5$.

2.7. *Neural network design and training*

We performed the neural network training and testing using MATLAB (The MathWorks, Inc., Natick, MA, USA). For each sEMG channel, the proposed algorithms were implemented using 200-sample (192 ms) sliding windows during the feature extraction process (fractal dimension, slope sign changes, waveform length and cepstral analysis). For each new pair of gyroscope sensor samples, estimates of updated Kalman-filter angular velocity (first proposed method) and knee joint angles (second and third proposed methods) were computed. For the first data fusion strategy, this approach resulted in a 19-coefficient feature vector per sample interval (6 cepstral coefficients, one fractal dimension coefficient, one slope sign changes coefficient and one waveform length coefficient per sEMG channel, plus one angular velocity coefficient). For the second and third strategies, we obtained 18-coefficient sEMG feature vector (6 cepstral coefficients, one fractal dimension coefficient, one slope sign changes coefficient and one waveform length coefficient per sEMG channel).

In all three strategies, the extracted features correspond to the inputs to a three-layer LM neural network. Each strategy used, 19 (first strategy) or 18 (second and third strategies) nodes in the input layer, 12 nodes in the hidden layer, and 1 node in the output layer (this output represents the estimated knee joint angle). We chose

the network's architecture and size empirically, aiming at the maximum possible reduction of the final mean squared error (MSE).

For neural network training, we used the same initial weight values for all three network layers (null weight for all neurons). The maximum number of iterations was 50, the stop criterion was MSE $< 10^{-10}\,\text{rad}^2$ (approximately $3.3 \times 10^{-7}\,\text{degrees}^2$), and the initial learning rate was 1. The actual joint angle measured with the electrogoniometer was used as training reference.

2.8. *Quantitative evaluation of the proposed methods and comparison with algorithms based solely on sEMG*

The proposed methods were compared with the following sEMG-only methods from the literature:

- recursive least squares method — LM neural network [Ferreira *et al.* (2005)]; this algorithm uses the AR model for feature extraction and a LM neural network for supervised learning.
- recursive least squares + histogram — self-organizing maps — LM neural network [Delis *et al.* (2009)]; this algorithm uses a combination of temporal and spectral domain approaches (signal amplitude histogram and AR coefficients, respectively) for feature extraction, and a feature projection stage with a self-organizing map and a LM neural network for supervised learning.
- energy of wavelet packet coefficients — principal components analysis — LM neural network (EWP-PCA) [Wang *et al.* (2006)]; this method uses the energy of the wavelet packet coefficients for feature extraction, principal components analysis for feature projection, and a LM neural network for supervised learning.

Note that the EWP-PCA algorithm was not originally designed to estimate intended knee joint angles for controlling active transfemoral leg prostheses. Given that we did not find in the literature an algorithm with a similar purpose, we adapted the EWP-PCA method to the myoelectric pattern recognition problem addressed in this work. We emphasize that the main components in the EWP-PCA approach, such as pattern recognition and order reduction, are relevant to the problems we face in the angle estimation issue, which justifies our comparisons.

For consistency, the myoelectric algorithms based solely on sEMG signals used the same LM network configuration, and also the same training process and test datasets. All algorithms were implemented using 200-sample (192 ms) windows with an overlapping approach, such that feature extraction was performed once for every new sEMG sample. Also, we used the same AR order and forgetting factor configuration for the proposed methods, and for the methods from Ferreira *et al.* [2005] and Delis *et al.* [2009].

For comparing all these methods, we used the 120 sets of sEMG, electrogoniometer, and gyroscope data that were not used during training. The performance of each algorithm was evaluated by comparing the knee angles estimated from the

sEMG signals with the joint angle values measured with the electrogoniometer. We applied a threshold over the time series to detect error events [Delis *et al.* (2009)] (this threshold was empirically set to 10°); each series of consecutive errors found to be above the threshold was considered an error event.

For performance evaluation, the myoelectric algorithms were quantitatively compared using statistical metrics based on: (i) the error-to-signal percentage; (ii) the correlation coefficient; (iii) the number of error events; and (iv) the maximum error amplitude [Delis *et al.* (2009)]. We evaluated these statistics for each set of sEMG signals, and computed, for each subject, the intra-subject mean and standard deviation (SD) of those parameters. Finally, since the values for the different participants are independent and based on the principles of error analysis [Taylor (1997)], we computed the inter-subject arithmetic averages of the intra-subject means (to obtain global means), and the inter-subject arithmetic averages of the participants' SDs (to obtain global SDs). The square root Mahalanobis distance was calculated for each metric as a means of assessing the statistical difference between the methods based solely on sEMG signals and the proposed methods [Delis *et al.* (2009); De Maesschalck *et al.* (2000)].

3. Results

In evaluating the proposed strategies, we first compare their results to the joint angle measurements obtained with the electrogoniometer. Then, we compare our results with those obtained using the methods from Ferreira *et al.* [2005], Delis *et al.* [2009] and Wang *et al.* [2006].

3.1. *Comparison with electrogoniometer measurements*

In Fig. 7, we present the knee joint angles estimated by the three proposed fusion-based algorithms, and the measurements from the electrogoniometer, for a representative study. The knee joint angles estimated by the proposed myoelectric algorithms strategies follow the angle provided by the electrogoniometer reasonably well, except for the occurrence of discrete artifacts, which, depending on their durations, may not affect the knee joint angle control.

3.2. *Comparison with methods from the literature*

Figure 8 illustrates the differences between the proposed myoelectric strategies and the methods from Ferreira *et al.* [2005], Delis *et al.* [2009] and Wang *et al.* [2006], for a representative set of measurements. Figures 8(a)–8(c) show knee angles estimated with the algorithms proposed in Ferreira *et al.* [2005], Delis *et al.* [2009] and Wang *et al.* [2006], respectively, as well as the absolute differences between the electrogoniometer measurements and the myoelectric estimates, for each case. Similarly, Figs. 8(d)–8(f) show the results obtained using the first, second, and third fusion-based approaches, respectively. Note that all the algorithms provided similar results, except of the EWP-PCA method, which produced less accurate results.

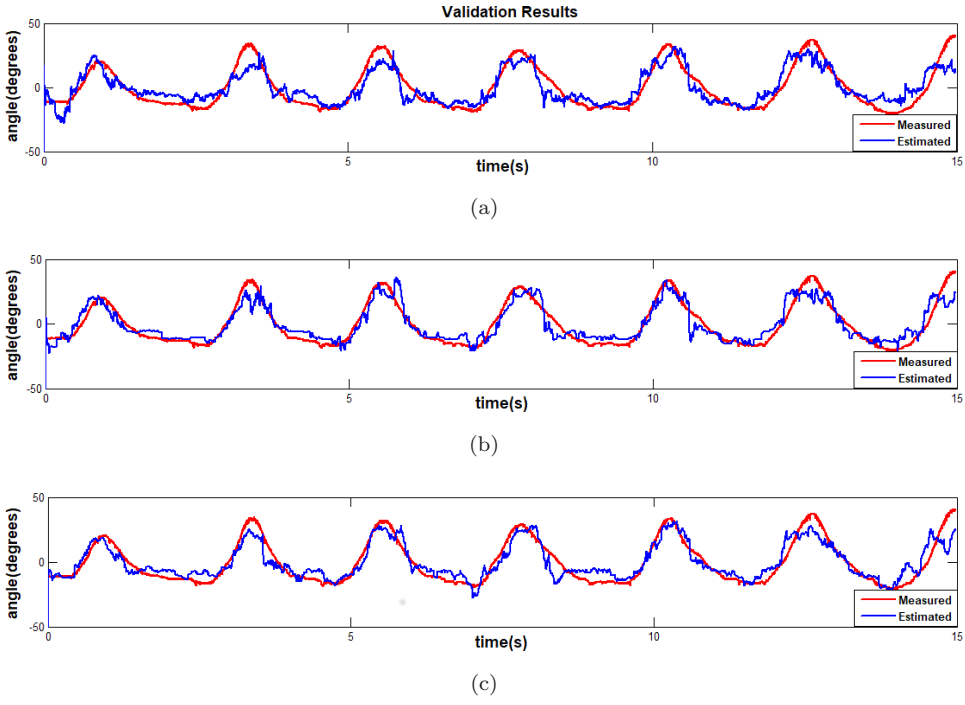

Fig. 7. Measured and estimated knee joint angles for the proposed algorithms: (a) first data fusion strategy; (b) second data fusion strategy; (c) third data fusion strategy.

Table 1 presents a quantitative comparison between the three proposed data fusion strategies and the methods from Ferreira *et al.* [2005], Delis *et al.* [2009] and Wang *et al.* [2006], concerning the previously described performance metrics: error-to-signal percentage, correlation coefficient, number of error events and maximum error amplitude. Mean and SD values correspond to global values, obtained as the inter-subject averages of the intra-subject mean and SD values, as described above.

These results suggest that the proposed data fusion strategies improve performance over the method Wang *et al.* [2006], concerning the error-to-signal percentage, the correlation coefficient, and maximum error amplitude. Furthermore, the second and the third proposed data fusion methods resulted in lower numbers of error events than the first data fusion method, and than the methods from Ferreira *et al.* [2005], Delis *et al.* [2009] and Wang *et al.* [2006]. The statistical significance of the above differences is evaluated in Tables 2–5, which are discussed below.

Table 2 presents the measured square root Mahalanobis distances between the results obtained with the first fusion-based strategy and the results obtained with the methods from Ferreira *et al.* [2005], Delis *et al.* [2009] and Wang *et al.* [2006] which are based solely on the sEMG signals. Note that, with 12 subjects, the results are considered to be statistically similar (with 95% confidence) if $d^2 \leq 21.03$,

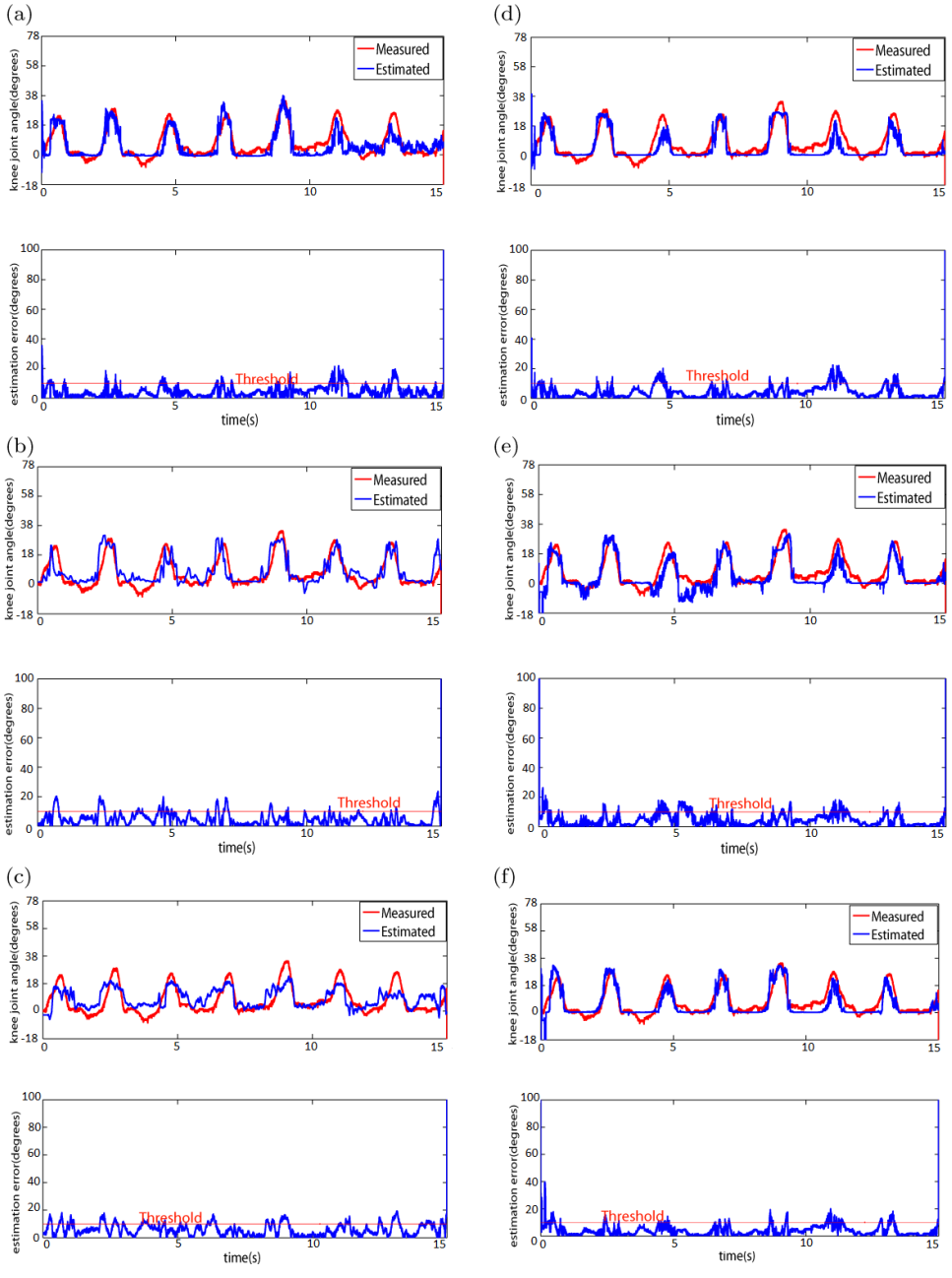

Fig. 8. Measured and estimated knee joint angles for two sets of signals taken from the same subject, using: (a) the algorithm from Ferreira *et al.* [2005]. (b) The algorithm from Delis *et al.* [2009]. (c) The algorithm from Wang *et al.* [2006]. (d) The first data fusion strategy. (e) The second data fusion strategy. (f) The third data fusion strategy.

Table 1. Performance metrics for the three proposed data fusion strategies and for algorithms based solely on sEMG signals (from the literature).

Performance metric	First data fusion strategy	Second data fusion strategy	Third data fusion strategy	Ferreira *et al.* [2005]	Delis *et al.* [2009]	Wang *et al.* [2006]
Error-to-signal percentage(%)	6.42 ± 1.82	6.58 ± 1.60	6.90 ± 2.37	6.75 ± 0.62	7.14 ± 0.53	10.14 ± 0.75
Correlation coefficient	0.86 ± 0.06	0.84 ± 0.06	0.81 ± 0.12	0.78 ± 0.04	0.75 ± 0.05	0.39 ± 0.07
Number of error events	32 ± 11	29 ± 7	29 ± 9.6	36.50 ± 3.71	27.00 ± 2.71	134.58 ± 13.97
Maximum error amplitude (degree)	35 ± 5	41 ± 12	36 ± 15	36.25 ± 3.16	36.67 ± 2.81	85.75 ± 14.20

Table 2. Square root Mahalanobis distance between the performance metrics obtained with the first data fusion strategy and those obtained with algorithms based solely on sEMG signals (from the literature).

Performance metric	Ferreira *et al.* [2005]	Delis *et al.* [2009]	Wang *et al.* [2006]
Error-to-signal percentage	1.02	1.61	4.86*
Correlation coefficient	1.09	1.59	5.89*
Number of error events	0.90	2.67	7.78*
Maximum error amplitude	19.11*	17.30*	5.09*
Maximum error event duration	1.97	0.90	2.48

*Statistically significant difference (with 95% confidence).

i.e. if $d \leq 4.58$. From the statistical significances, we found that all the metric statistics were equivalent to those obtained with the methods from Ferreira *et al.* [2005] and Delis *et al.* [2009], except the maximum amplitude error, for which our first fusion-based method yielded significantly lower results. In comparison with the EWP-PCA algorithm, on the other hand, the first proposed strategy lead to significantly lower error-to signal percentage, correlation coefficient, number of error events and maximum amplitude error, while the results are statistically equivalent concerning to the maximum error event duration.

Similarly, Tables 3 and 4 present the measured square root Mahalanobis distances between the results obtained with the second and third fusion-based strategies, respectively, and the results obtained with the methods from the literature. We found that the results obtained with the second and third data fusion strategies

Table 3. Square root Mahalanobis distance between the performance metrics obtained with the second data fusion strategy and those obtained with algorithms based solely on sEMG signals (from the literature).

Performance metric	Ferreira *et al.* [2005]	Delis *et al.* [2009]	Wang *et al.* [2006]
Error-to-signal percentage	0.52	1.00	4.37
Correlation coefficient	0.84	1.37	5.78*
Number of error events	1.82	1.33	8.25*
Maximum error amplitude	1.24	1.27	3.41
Maximum error event duration	2.16	0.87	2.27

*Statistically significant difference (with 95% confidence).

Table 4. Square root Mahalanobis distance between the performance metrics obtained with the third data fusion strategy and those obtained with algorithms based solely on sEMG signals (from the literature).

Performance metric	Ferreira *et al.* [2005]	Delis *et al.* [2009]	Wang *et al.* [2006]
Error-to-signal percentage	0.98	1.53	4.58
Correlation coefficient	0.90	1.37	5.83*
Number of error events	1.80	1.21	8.27*
Maximum error amplitude	0.96	1.07	3.57
Maximum error event duration	2.20	0.85	2.02

*Statistically significant difference (with 95% confidence).

Table 5. Square root Mahalanobis distance between the performance metrics obtained with the three proposed data fusion strategies.

Performance metric	First versus second	First versus third	Second versus third
Error-to-signal percentage	0.73	0.87	1.03
Correlation coefficient	0.67	0.78	0.76
Number of error events	1.64	1.78	0.78
Maximum error amplitude	20.60*	14.86*	1.38
Maximum error event duration	0.86	0.78	1.04

*Statistically significant difference (with 95% confidence).

do not differ significantly from the results obtained with the methods from Ferreira *et al.* [2005] and Delis *et al.* [2009]. In comparison with the EWP-PCA method [Wang *et al.* (2006)], our second and third methods provided significantly different results concerning the correlation coefficient and the number of error events; the results are nevertheless equivalent concerning the error-to-signal percentage, maximum amplitude, and error event duration.

3.3. *Comparison between the proposed strategies*

Table 5 shows the measured square root Mahalanobis distances between the results obtained with the proposed fusion-based methods. We found that the maximum amplitude error associated with the first strategy is significantly lower than those provided by the second and third strategies. We also found that the results obtained with the second and third strategies are equivalent with respect to all the evaluated metrics.

3.4. *Evaluation of the robustness to movement artifacts*

Figure 9(a) shows a sEMG signal with movement artifacts, along with measured knee joint angles. Figures 9(b)–9(d) show the measured and estimated joint angles for the same set of signals, as estimated by the sEMG-based algorithms from Ferreira *et al.* [2005], Delis *et al.* [2009] and Wang *et al.* [2006], respectively, as well as the absolute differences between these estimates and the measured angles. Similarly, Figs. 9(e)–9(g) compare the measured values with those estimated with the three proposed fusion-based approaches. False positives were observed on the results obtained with the methods from Ferreira *et al.* [2005] and Delis *et al.* [2009], and with the three proposed methods. The EWP-PCA algorithm was not able to estimate the joint angle from these data (Fig. 9(d)). Qualitatively, the best results were obtained with the third proposed strategy. These results suggest that this approach may be more robust to movement artifacts.

3.5. *Evaluation of the robustness to 60 Hz interference*

The results shown in Fig. 10 are related to the robustness of the algorithms to 60 Hz interference. Figure 10(a) shows a sEMG signal added with artificial 60 Hz

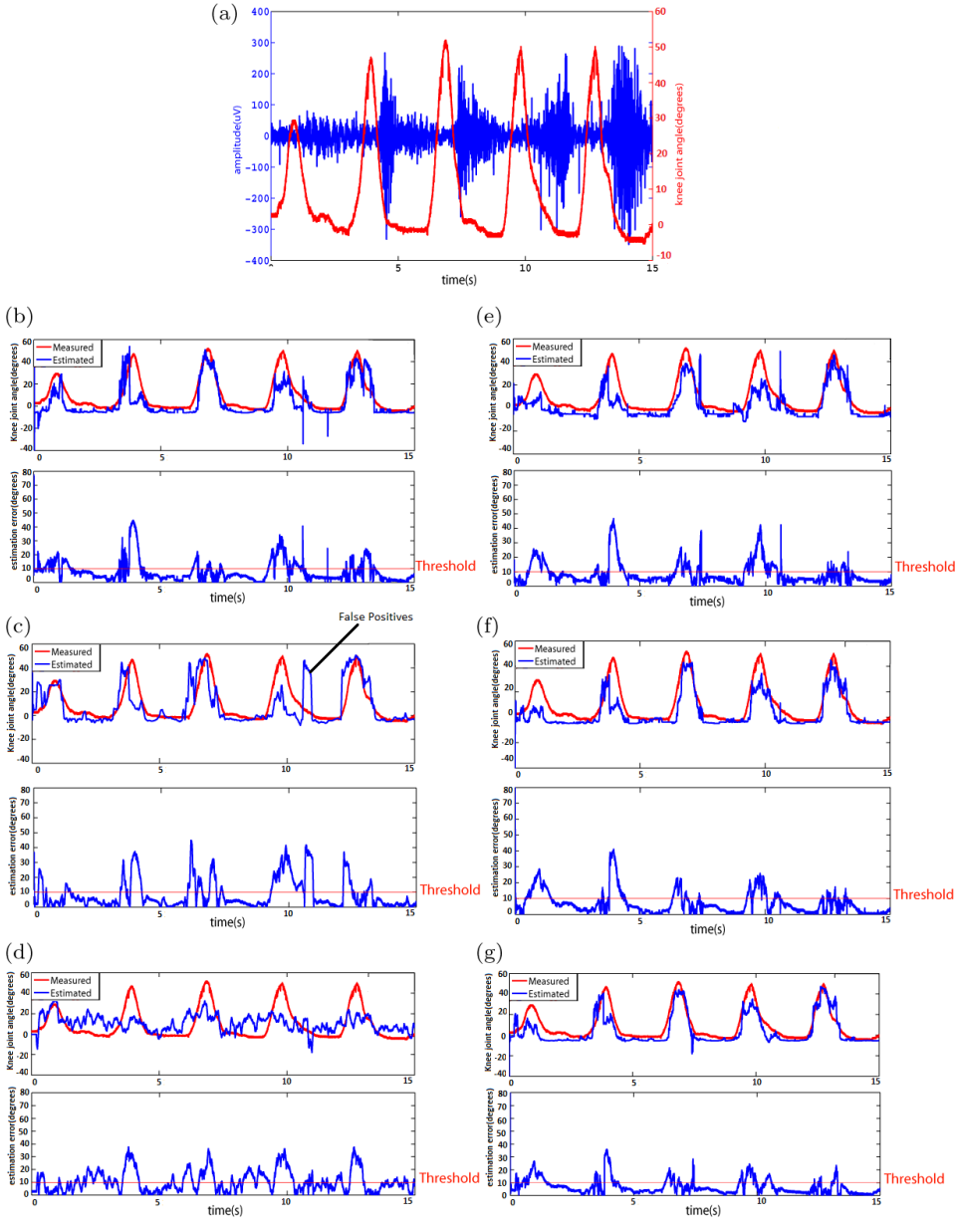

Fig. 9. Qualitative evaluation of the algorithms' robustness to movement artifacts. (a) sEMG signal with movement artifacts, and measured knee angles. Knee angles (and corresponding absolute errors) estimated using: (b) the algorithm from Ferreira *et al.* [2005]. (c) The algorithm from Delis *et al.* [2009]. (d) The algorithm from Wang *et al.* [2006]. (e) The first data fusion strategy. (f) The second data fusion strategy. (g) The third data fusion strategy.

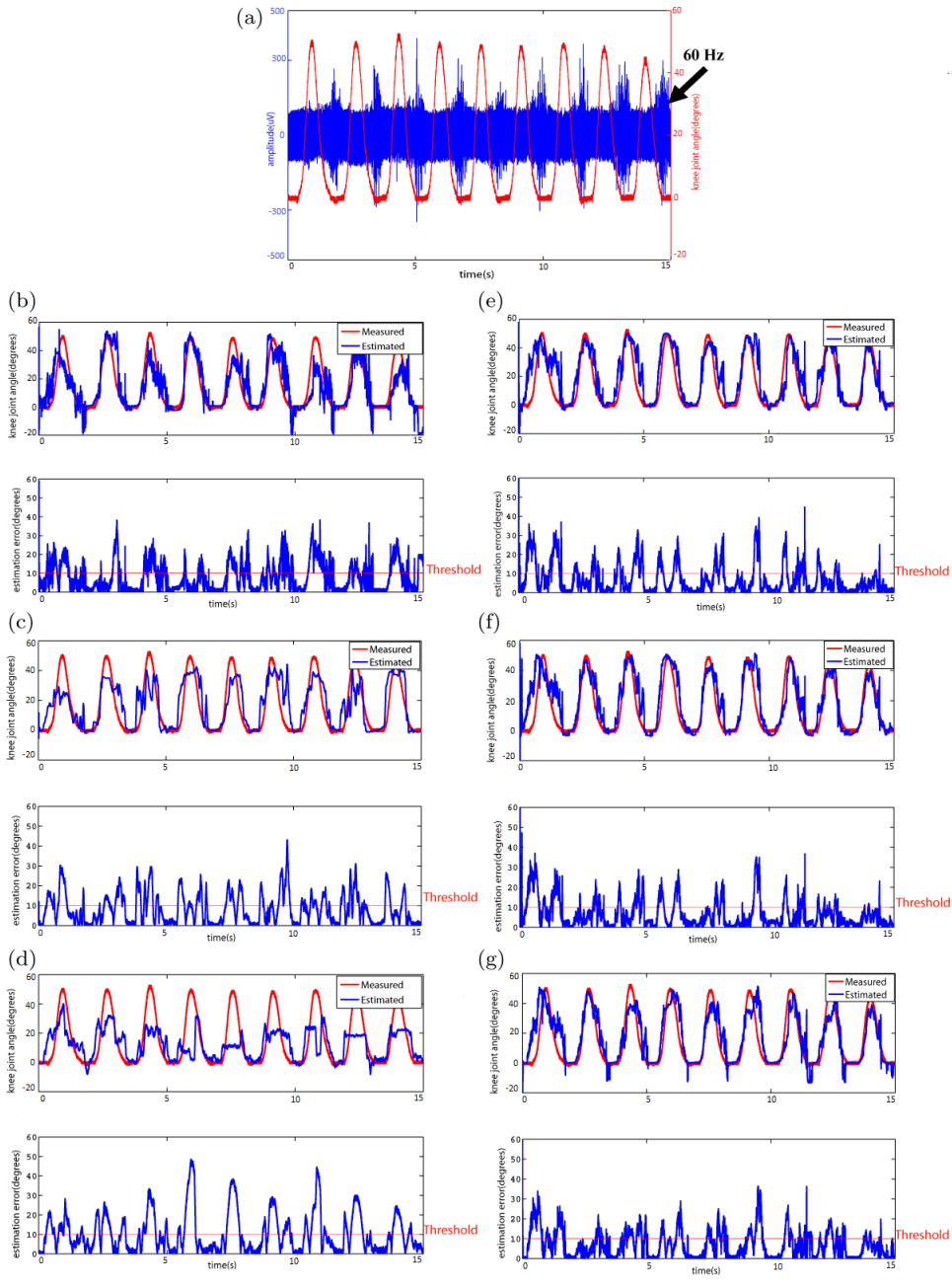

Fig. 10. Qualitative evaluation of the algorithms' robustness to 60 Hz power line interference. (a) sEMG signal with added artificial 60 Hz interference, and measured knee angles. Knee angles (and corresponding absolute errors) estimated using: (b) the algorithm from Ferreira *et al.* [2005]. (c) The algorithm from Delis *et al.* [2009]. (d) The algorithm from Wang *et al.* [2006]. (e) The first data fusion strategy. (f) The second data fusion strategy. (g) The third data fusion strategy.

interference, along with measured knee joint angles. Figures 10(b), 9(c), and 9(d) show the measured and estimated joint angles for the same set of signals, as estimated by the SEMG-based algorithms from Ferreira *et al.* [2005], Delis *et al.* [2009] and Wang *et al.* [2006], respectively, as well as the absolute differences between these estimates and the measured angles. Similarly, Figs. 10(e), 9(f), and 9(g) compare the measured values with those estimated with the three proposed fusion-based approaches. The EWP-PCA algorithm (Fig. 10(d)) was able to somewhat follow the knee joint motion, but the estimated angles differed considerably from the measured values. All other methods were able to track the knee joint movement reasonably well, but we found that the proposed data fusion strategies provided slightly better results than those provided by the methods based solely on the sEMG data.

4. Discussion

The quantitative analysis of the experimental results shows that the first proposed data fusion strategy leads to a statistically significant reduction of the maximum amplitude of error, when compared with the methods from Ferreira *et al.* [2005], Delis *et al.* [2009] and Wang *et al.* [2006]. We attribute this difference to the data fusion, in the LM neural network, between the extracted features (fractal dimension, slope sign changes, waveform length and cepstral coefficients) and the inertial signals. In fact, this fusion reduces the noise in the estimated knee joint angle, due to the use of a Kalman-filter, which, in this application, is equivalent to a low-pass filter with time-varying cut-off frequency.

The proposed strategies showed significantly better results than the EWP-PCA myoelectric algorithm [Wang *et al.* (2006)]. A possible explanation for these results could be that PCA analysis minimizes the redundancy among the feature vectors, and does not take into account the relationship between these vectors and the myoelectric classes during the estimation procedure. Furthermore, time domain and AR features have been shown to outperform time-frequency features for stationary or slowly changing data, and to provide equivalent results for steady-state sEMG signals [Huang *et al.* (2005)].

The proposed fusion-based algorithms showed an improved performance with respect to 60 Hz interference, when compared with methods based solely on sEMG data (see Fig. 10). The observed error peaks may be caused by noise in the feature space, and by an insufficient number of neurons in the LM network's hidden layer. This problem may be addressed by increasing the number of neurons, by increasing the number of sEMG channels and by increasing the length of the sliding window used in the fractal dimension, slope sign changes, waveform length and cepstral coefficients analyses. However, these approaches would result in increased computational complexity and convergence time, and could increase the response time of the prosthesis.

The addition of other variables associated with leg proprioception may improve the precision and reduce artifacts, without significantly increasing the computational complexity of the myoelectric algorithms.

The three proposed strategies incur equivalent computational costs. Quantitatively, the first proposed strategy provided better performance concerning the maximum amplitude of error event, when compared with the second and third proposed strategies. This improvement may be significant when error events that are long enough to be noticed by the leg prosthesis occur, especially if these error events cause the joint estimation to exceed the workspace limits. On the other hand, the third proposed strategy seems to be more robust to movement artifacts than all other evaluated methods. In this work, the main objective was demonstrating that is possible the continue estimation prediction the angle for a transfemoral leg prostheses. In first instance, the proposals algorithms based on data fusion was tested in off-line mode without evaluated the complexity of framework and aspects as time-response during the testing process. In future work, will be evaluated the proposals algorithms in on-line mode as well as the complexity aspects of the framework to implement an optimization toolbox.

The data fusion configuration associated with the correction process in the Kalman-filter, combined with a statistical distance test, provides better performance when poor electrode contact or sudden changes in the electrode–electrolyte interface are observed. The latter is common in fatigue processes. With an appropriate calibration of the gyroscope sensors, the orientation estimate diverges at most 1 degree every 10 s. Therefore, in case of a long-duration fault in the sEMG acquisition system, the joint angle estimation algorithm would have time to detect and correct these problems. This joint angle correction capability makes the third method the most appropriate amongst all evaluated strategies.

5. Conclusion

This work introduced three variants of a myoelectric algorithm for estimating intended knee joint angles using the data fusion of surface electromyographic and inertial signals. The estimated angles may provide the information needed to control active transfemoral leg prostheses.

Our experimental results suggest that the proposed methods result in statistically significant improvements with respect to the EWP-PCA method. Furthermore, they showed an increased robustness with respect to 60 Hz noise and to movement artifacts, in comparison with methods based solely on sEMG data. Quantitatively, the first proposed strategy provided better performance with respect to the maximum amplitude of error event. This improvement may be significant when error events that are long enough to be noticed by the leg prosthesis occur. On the other hand, the third proposed strategy seems to be more robust to movement artifacts than all other evaluated methods.

In future works, we will include other sensors on the patient's body, such as accelerometers, magnetometers and pressure sensors in the shoes. These will further

aid parameter estimation, and therefore improve the prosthesis performance. The data fusion concepts we used in our algorithms may be useful in the development of an algorithm in which signals from many different sensors are fused and used in the development of a predictive movement model.

Acknowledgments

This work was financially supported by a grant from the Brazilian Ministry of Education — MEC/CAPES — and by a productivity and postdoctoral fellowship from the National Council for Technological and Scientific Development — CNPq.

References

Acharya, R. U., Bhat, P. S., Kannathal, N., Rao, A. and Lim, C. M. (2005). Analysis of cardiac health using fractal dimension and wavelet transformation. *ITBM-RBM* 2005, **26**: 133–139.

Ahlstrom, M. L. and Tompkins, W. J. (1985). Digital filters for real-time ECG signal processing using microprocessor. *IEEE Trans. Biomed. Eng.*, **32**: 708–713.

Chiou, Y., Luh, J., Chen, S., Lai, J. and Kuo, T. (2004). The comparison of electromyographic pattern classifications with active and passive electrodes. *Med. Eng. Phys.*, **26**, 7: 605–610.

Dasarathy, B. V. (1997). Sensor fusion potential exploitation-innovative architectures and illustrative applications. *Proceedings IEEE*, pp. 24–38.

De Maesschalck, R., Jouan-Rimbaud, D. and Massart, D. L. (2000). The Mahalanobis distance. *Chem. Intell. Lab. Syst.*, **50**: 1–18.

Delis, A. L., Carvalho, J. L. A., da Rocha, A. F., Ferreira, R. U., Rodriguez, S. S. and Borges, G. A. (2009). Estimation of the knee joint angle from surface electromyographic signals for active control of leg prostheses. *Physiol. Measure.*, **30**: 931–946.

Diniz, P. S. R. (1997). *Adaptive Filtering Algorithms and Practical Implementation*. Kluwer Academic Publishers.

Duda, R. O., Hart, P. E. and Stork, D. G. (2000). *Pattern Classification*, 2nd edn. Wiley, New York.

Esteller, R., Vachtsevons, G., Echautz, J. and Litt, B. (2001). A comparison of waveform fractal dimension algorithms. *IEEE Trans. Circuit Syst., Fundamental Theory Appl.*, **48**, 2: 177–183.

Fan, Y. and Yin, Y. (2013). Active and progressive exoskeleton rehabilitation using multisource information fusion from EMG and force-position EPP. *IEEE Trans. Biomed. Eng.*, **60**, 12: 3314–3321.

Ferreira, R. U., da Rocha, A. F., Cascão, C. A. Jr., Borges, G. A., Nascimento, F. A. O. and Veneziano, W. H. (2005). Reconhecimento de padrões de sinais de EMG para controle de prótese de perna. *Proc. XI Congresso Brasileiro de Biomecânica.*

Fukuda, O., Tsuji, T., Kaneko, M. and Otsuka, A. (2003). A human assisting manipulator teleoperated by EMG signals and arm motions. *IEEE Trans. Robot Autom.*, **19**: 210–222.

Grimes, D. L., Flowers, W. C. and Donath, M. (1977). Feasibility of an active control scheme for above knee prostheses. *J. Biomech. Eng.*, **99**: 215–221.

Gupta, V. and Reddy, N. P. (1996). Surface electromyogram for the control of anthropometric teleoperator fingers Medicine Meets Virtual Reality. *Healthcare in the*

Information Age (IOP Press Amsterdam Weghorst SJ Sieburg HB Morgan KS), pp. 482–487.

Ha, K., Varol, H., H. A. and Goldfarb, M. (2011). Volitional control of a prosthetic knee using surface electromyography. *IEEE Trans. Biomed. Eng.*, **58**: 144–151.

Hagan, M. T. and Menhaj, M. B. (1994). Training feedforward networks with the Marquardt Algorithm. *IEEE Trans. Neural Net.*, **5**, 6: 989–993.

Hall, D. L. and Llinas, J. (1997). An introduction to multisensor data fusion. *Proceed. IEEE*, pp. 6–23.

Higuchi, T. (1998). Approach to irregular time series on the basis of the fractal theory. *Physica D*, **31**: 277–283.

Hu, X., Wang, Z. and Ren, X. (2005). Classification of surface EMG signal with Fractal dimension. *J. Zhejiang Univ. Sci.*, **6B**, 8: 844–848.

Huang, Y., Englehart, K. B., Hudgins, B. and Chan, A. D. C. (2005). A Gaussian mixture model based classification scheme for myoelectric control of powered upper limb prostheses. *IEEE Trans. Biomed. Eng.*, **52**, 11: 1801–1811.

Ito, K., Tsukamoto, M. and Kondo, T. (2008). Discrimination of intended movements based on Nonstationary EMG for a prosthetic hand control. *Proceedings the ISCCSP*, pp. 14–19.

Kang, W. J., Shiu, J. R., Cheng, C. K., Lai, J. S. and Tsao, H. W. (1995). The application of cepstral coefficients and maximum likelihood method in EMG pattern recognition. *IEEE Trans. Biomed. Eng.*, **42**: 777–785.

Kastner, J., Nimmervoll, R. and Wagner, I. P. (1999). What are the benefits of the Otto Bock Cleg? A comparative gait analysis of C-leg, 3R45 and 3R80. *J. Med. Orthopedic*, **119**: 131–137.

Lizhi, P., Dingguo, Z., Jianwei, L., Xinjun, S. and Xiangyang, Z. (2014). Continuous estimation of finger joint angles under different static wrist motions from surface EMG signals. *Biomed. Signal Process. Control*, **14**: 265–271.

López, N. M., di Sciascio, F., Soria, C. M. and Valentinuzzi, M. E. (2009). Robust EMG sensing system based on data fusion for myoelectric control of a robotic arm. *Biomed. Eng. Online*, **8**,5.

Luo, R. C. (1996). Sensor technologies and microsensor issues for mechatronics system. *IEEE/ASME Trans. Mechatron*, **1**: 39–49.

Luo, R. C., Yih, Ch. and Su, K. L. (2002). Multisensor fusion and integration: Approaches, applications, and future research directions. *IEEE Sensor*, **2**: 107–119.

Manyika, J. and Durrant-Whyte, H. (1994). *Data Fusion and Sensor Management*: *A Descentralized Information* — Theoretic Approach, Ellis Horwood, London.

Merletti, R. and Parker, P. A. (2009). *ELECTROMYOGRAPHY Physiology*, *Engineering*, *and Noninvasive Applications*, IEEE Press Engineering in Medicine and Biology Society.

Oskoei, M. A. and Hu, H. (2007). Myoelectric control system — A survey. *Biomed. Signal Process. Control*, **2**: 275–294.

Phinyomark, A., Phukpattaranont, P. and Limsakul, Ch. (2012). Feature reduction and selection for EMG signal classification. *Expert Syst. Appl.*, **39**: 7420–7431.

Popovic, D., Oguztorelli, M. N. and Stein, R. B. (1995). Optimal control for an above-knee prosthesis with two degrees of freedom. *J. Biomech.*, **28**: 89–98.

Reddy, N. P. and Gupta, V. (2007). Toward direct biocontrol using surface EMG signals: Control of finger and wrist joint models. *Med. Eng. Phys.*, **29**: 398–403.

Sawaguchi, E., Sadahiro, T. and Iwase, M. (2011). Wrist angle estimation based on Musculoskeletal systems with EMG. *6th IEEE Int. Conf. Intelligent Data Acquisition*

and Advanced Computing Systems: *Technology and Applications*, 15–17 September, Prague, Czech Republic, pp. 269–276.

Shengxin, W., Yongsheng, G., Jie, Z., Tao, Y. and Yanhe, Z. (2017). Prediction of sEMG-based tremor joint angle using the RBF neural network. *Proc. 2012 IEEE Int. Conf. Mechatronics and Automation*, pp. 2103–2108.

SENIAM, (2008). Surface Electromyography for Noninvasive Assessment of muscle, http://www.seniam.org.

Silva, J., Chau, T. and Goldenberg, A. (2003). MMG-based multisensor data fusion for prosthesis control. *Proc. IEEE CMBS*, pp. 2909–2912.

Smith, R. J., Tenore, F., Huberdeau, D., Etiene-Cummings, R. and Thakor, N. V. (2008). Continuous decoding of finger position from surface EMG signals for the control of powered prostheses. *Proc. 2008 IEEE/EMBC 30th Annual Int. Conf. Engineering in Medicine and Biology Society*, pp. 2393–2396.

Surynarayanan, S. and Reddy, N. P. (1997). EMG based interface for position tracking in VR environments and telemanipulation presence. *Teleoperators Virtual Environ.*, **6**: 282–291.

Sup, F., Bohara, A. and Goldfarb, M. (2008). Design and control of a powered transfemoral prosthesis. *Int. J. Robot. Res.*, **27**, 2: 263–73.

Sup, F., Varol, H. A., Mitchell, J., Withrow, T. and Goldfarb, M. (2008a). Design and control of an active electrical knee and ankle prosthesis. *Proc. 2nd Biennial IEEE/RAS-EMBS Int. Conf. Biomedical Robotics and Biomechatronics*, pp. 523–528.

Tang, Z., Zhang, K., Sun, S., Gao, Z., Zhang, L. and Yang, Z. (2014). An upper-limb power-assist exoskeleton using proportional myoelectric control. *Sensors* **14**: 6677–6694.

Taylor, J. R. (1997). *An Introduction to Error Analysis — The Study of Uncertainties in Physical Measurements*, 2nd edn. Sausalito, California, University Science Books.

Wang, G., Wang, Z., Chen, W. and Zhuang, J. (2006). Classification of surface EMG signals using optimal wavelet packet method based on Davies–Bouldin criterion. *Med. Biol. Eng. Comput.*, **44**: 865–872.

Yang, Ch., Xingang, Z. and Jianda, H. (2013). Hierarchical projection regression for online estimation of elbow joint angle using EMG signals. *Neural. Comput. Appl.*, **23**: 1129–1138.

Zhang, F., Li, P., Hou, Z., Lu, Z., Chen, Y., Li, Q. and Tan, M. (2012). sEMG-based continuous estimation of joint angles of human legs by using BP neural network. *Neurocomput. J.*, **78**: 139–148.